Journal of Colloid and Interface Science 542 (2019) 159–167

Contents lists available at ScienceDirect

Journal of Colloid and Interface Science

journal homepage: www.elsevier.com/locate/jcis

Regular Article

Solvent-free graphene liquids: Promising candidates for lubricants without the base oil

Jiaoxia Zhang [a,1,*], Peipei Li [b,1], Zhuangzhuang Zhang [a], Xiaojing Wang [a], Jijun Tang [a], Hu Liu [c,d], Qian Shao [e], Tao Ding [f,*], Ahmad Umar [g,*], Zhanhu Guo [c,*]

[a] School of Materials Science and Engineering, Jiangsu University of Science and Technology, Zhenjiang 212003, China
[b] School of Advanced Materials and Nanotechnology, Xidian University, Xi'an, Shaanxi 710071, China
[c] Integrated Composites Laboratory (ICL), Department of Chemical & Biomolecular Engineering, University of Tennessee, Knoxville, TN 37996, USA
[d] Key Laboratory of Materials Processing and Mold (Zhengzhou University), Ministry of Education, National Engineering Research Center for Advanced Polymer Processing Technology, Zhengzhou University, Zhengzhou 450002, China
[e] College of Chemical and Environmental Engineering, Shandong University of Science and Technology, Qingdao, Shandong 266590, China
[f] College of Chemistry and Chemical Engineering, Henan University, Kaifeng 475004, China
[g] Department of Chemistry, Faculty of Sciences and Arts, Promising Centre for Sensors and Electronic Devices (PCSED), Najran University, P.O. Box 1988, Najran 11001, Saudi Arabia

GRAPHICAL ABSTRACT

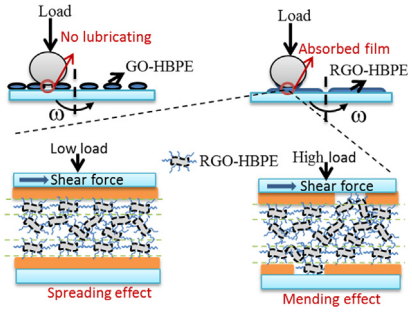

ARTICLE INFO

Article history:
Received 2 November 2018
Revised 30 January 2019
Accepted 31 January 2019
Available online 1 February 2019

Keywords:
Graphene oxide
Hyperbranched polyamine-ester
Solvent-free graphene liquids
Lubricant

ABSTRACT

Reduced graphene oxide modified by hyperbranched polyamine-ester (RGO-HBPE) liquids was successfully fabricated through the surface chemical engineering and tested for serving as a solvent-free novel lubricant. Structural characterization, dispersibility and rheology behavior of the lubricant and the related frication performance on steel plate were investigated thoroughly. The results manifest that the RGO-HBPE exhibited good dispersity in distilled water and liquid behavior without any solvent at ambient temperature. And this RGO-HBPE liquids could be directly introduced onto the surface of steel plate as lubricants without any additional base oil. Tribological results and the proposed lubricating mechanism of RGO-HBPE imply that the fluidity of RGO-HBPE is favorable for lubrication and is crucial to reduce the friction coefficient. The spontaneous flow of RGO-HBPE provide a spreading effect to form the lubricating film. The specific spreading effect of RGO-HBPE and the synergistic lubricating effect between HBPE and graphene demonstrate that RGO-HBPE could be directly used as promising candidates for lubricants in nowadays moving machines.

* Corresponding authors.
E-mail addresses: zhangjx@just.edu.cn (J. Zhang), dingtao@henu.edu.cn (T. Ding), ahmadumar786@gmail.com (A. Umar), zguo10@utk.edu (Z. Guo).
[1] J. Zhang and P. Li contributed equally to this work.

https://doi.org/10.1016/j.jcis.2019.01.135
0021-9797/

1. Introduction

Traditional lubricants face challenges of minimizing both frictional coefficient and moving mechanical damages [1,2]. Novel lubricant materials have been developed to overcome those problems [3–5]. Generally, traditional solid lubricants, such as graphite and molybdenum sulphide, are used as additive and introduced into the base oil to improve antifriction and antiwear properties [6,7]. Unlike solid lubricants, liquid lubricants possess more obvious advantages such as a lower machinery noise, longer term endurance, and more favorable thermal conductance in the elastohydrodynamic regime [8]. However, both solid and liquid lubricants exhibit the deficiency of themselves [9]. For example, solid additives are easy to agglomerate owing to both large specific surface areas and their poor compatibility with some liquid medium [10]. Though liquid lubricating oil is convenient to use directly, the wear resistance is reduced due to the soft chain and weak bond of the molecules. Thus, it is essential to explore a novel lubricating system which combines the advantages of both solid and liquid lubricants, and simultaneously avoids their deficiencies. For example, Giannelis et al. had developed solvent-free liquids, i.e., core nanoparticles grafted with organic oligomers [11,12]. In this hybrid system, the organic oligomers acted as a fluid medium to warrant fluidity, while the core nanoparticles were adjusted according to the demanded function [13,14].

Additionally, in the last decades, solvent-free nanofluids or liquids combining the fluidity and designability supply a desired platform for specific applications [11,15–20]. For example, graphene oxide/zinc hydroxystannate nanoparticles successfully served as flame retardant [21,22]. For gas separation, the cavities of hollow silica and the organic oligomeric chains served as gas transport pathway and a separation medium, respectively [13,23]. As for the lubricating materials, Archer et al. had demonstrated that the obtained solvent-free silica-based poly-alpha-olefin (PAO) fluids displayed a better lubricant behavior than PAO [24]. Most importantly, these lubricants also improved the wear resistance due to the supporting silica in the wear trails [12,24]. Namely, the solvent-free liquids, one of the ideal lubricating systems, combines the advantages of both liquid and solid lubricants. Although, current researches mainly focus on solvent-free liquids as lubricating additives, it's worth for the solvent-free liquids to be directly used as lubricants having the same results as the base oil.

Graphene displays a hexagon lattice of graphitic materials [3,21,25,26]. Its excellent thermal/electrical conductivity [27,28] and lubricating properties attract many interests in different fields [1,25,29–31]. Graphene platelets have served as additives to resist the friction and wear at an optimal concentration [30,32,33]. Moreover, previous reports imply that graphene as a self-lubricant can reduce friction-related energy and corresponding losses in different tribological applications [3,34]. Therefore, the solvent-free graphene liquids are expected to work as promising candidates for lubricants without any base oil, which has not been reported yet.

In this study, GO was synthesized based on a modified Hummers method [21,35,36]. The solvent-free graphene liquids (RGO-HBPE) were successfully fabricated according to the surface grating of GO with hyperbranched polyamine-ester (HBPE). Their structure, solubility in water, and rheology behavior were characterized, and the lubricant properties of RGO-HBPE on metal plates were analyzed. Besides, the lubricant properties of blank metal plates and GO-HBPE on metal plates were also performed to compare the effects of fluidity behavior of RGO-HBPE and the applied load. At the end, the frictional surfaces of the samples were observed to deduce the antifriction and lubricating mechanisms for these solvent-free graphene liquids.

2. Experimental section

2.1. Materials

The natural graphite, HCl (36–38%), H_2SO_4 (95–98%), $N_2H_4{\cdot}H_2O$ (30%), and $KMnO_4$ were purchased from Sinopharm Chemical Reagent. Deionized (DI) water was obtained with Ulupure ultrapure water device. The hyperbranched polyamine-ester (HBPE) was synthesized by SN_2 nucleophile substitution reaction based on the AB_2 branched monomer (see Fig. S1) [37].

2.2. RGO-HBPE and GO-HBPE nanomaterials

As shown in Fig. 1, graphite oxide was obtained based on the oxidation of natural graphite [21]. Then, 140 mL DI water and 1.4 g graphite oxide were introduced in 3-neck flask to ultrasonically treat for 1 h. Previously prepared HBPE (5 g) was transferred into the above 3-neck flask and sonicated for 0.5 h. Subsequently, $N_2H_4{\cdot}H_2O$ (2 g) was dropped into the 3-neck flask under stirring [36]. For completely reducing GO, the 3-neck flask was performed under magnetically stirring at 60 °C for 6 h. The suspension was centrifuged to collect the precipitate, then rinsed for several times with DI water, and dried to finally form the RGO-HBPE sample. For comparison, the GO-HBPE nanomaterials were also fabricated using the same treatment in the absence of $N_2H_4{\cdot}H_2O$.

2.3. Characterizations

The Fourier transform infrared spectroscopy (FTIR) was chosen to characterize the synthesized products on WQF-310 spectrometer with dry KBr tablet. The Raman spectra were executed to determine the structure variation of the synthesized products by the confocal Raman microscope (Invia Renishaw) with a 514 nm laser excitation source. The rheometer tracking their rheological behaviors by TA Instruments (ARG2) was employed at a 10 rad/s of angle frequency, 2.0% of strain amplitude and the 30–65 °C of temperature range. The heat stability of the samples was taken by a thermo-gravimetric analysis (TGA) measurement (Q50 TA) with a heating rate of 10 °C per min using a nitrogen protection (at a flow rate of 20 mL/min). Worn surfaces and roughness were characterized by the confocal laser scanning microscopy (LEXTOL S4000).

The ultraviolet spectrophotometer (UV–vis) was adopted to evaluate the dispersion of GO-HBPE and RGO-HBPE in water. The sample solutions with different concentrations were scanned based on DI water as a reference solution. According to the intensity versus concentration, the linear calibration curve was depicted (see Fig. S2). Subsequently, the supernatant liquor after depositing different time intervals was scanned to affirm their concentration and evaluate their dispersion.

Tribological studies of the steel plate samples coated with GO-HBPE and RGO-HBPE against counterface balls were implemented by the friction wear testing machine (UMT-2) with a ball-on-disk contact pattern at room temperature in air. Firstly, the 304-grade stainless steel plate samples (10 * 10 mm) were grounded with sand paper and polished with 0.5 μm abrasive paste. Then they were cleaned by acetone and methanol through sonication to remove residues. At last, the plates were carefully coated with equal amount of GO-HBPE or RGO-HBPE for comparison, respectively. The Al_2O_3 (2055 HV_1) balls were used as counterface balls. The applied load during the tribotest changed from 1 to 3 N at a speed of 25 mm/s, and the wear track radius was 0.5 mm for 30 min. The tests for each load were repeated for three times to obtain mean friction coefficients. In addition, the blank steel plate sample was also performed for comparison.

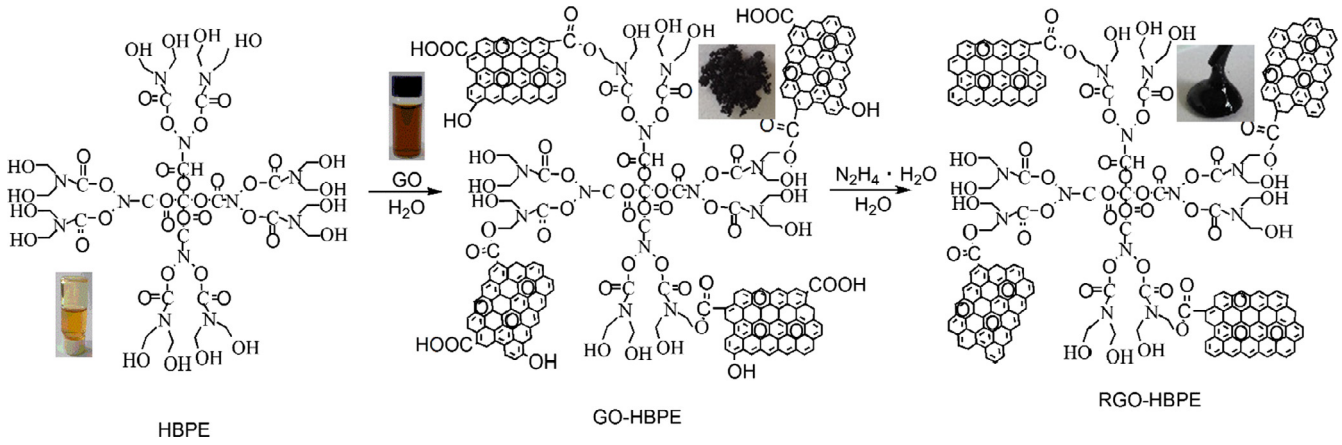

Fig. 1. Synthetic schematic of RGO-HBPE.

3. Results and discussion

3.1. Structural analysis

Fig. 2a shows the FTIR spectra of GO, GO-HBPE and RGO-HBPE. In the case of GO (Fig. 2a), the appearance of peak from 1620 to1720 cm^{-1} is the stretching of C═O bond. In addition, an observed band at 3440 cm^{-1} indicates the stretching OH, and the stretching C—O occurs at 1195 cm^{-1}. Epoxy bond results in a faint peak at around 900 cm^{-1} [38–40]. Thus, those oxygenic groups are introduced onto the surface of GO. The bands of OH stretching vibration for the RGO-HBPE and GO-HBPE exhibit intensifier and broader peaks owing to a large amount of OH in the HBPE. The C═O peak shifts to 1589 cm^{-1} due to the inductive effect and weak bond of HBPE. The new peak at about 1406 cm^{-1} is associated with the C—O vibration of carboxyl. The C—N vibration contributes to the band around 1072 cm^{-1}. The results are further verified with the XPS analysis (Fig. S3).

Raman spectra are used to explore the layered and defect structure of graphene materials [41,42], as shown in Fig. 2b. The two bands around 1350 (D) and 1590 cm^{-1} (G) reflect the disorder, symmetry and crystallization, respectively. A bigger intensity ratio of the D versus G band (I_D/I_G) represents more defects for carbon materials [39,43–46]. Compared with the GO ($I_D/I_G = 0.91$), I_D/I_G

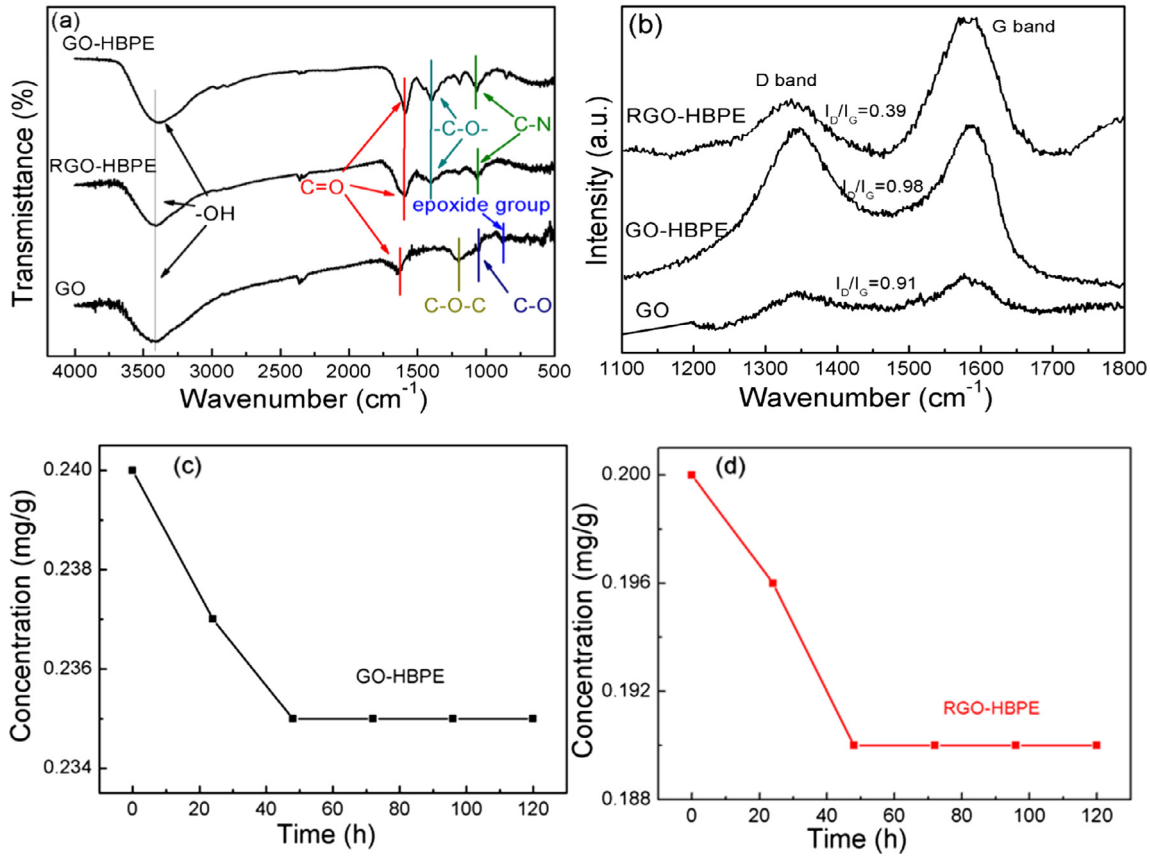

Fig. 2. (a) FTIR spectra, (b) Raman spectra of GO, GO-HBPE and RGO-HBPE; curves of concentration versus time for (c) GO-HBPE and (d) RGO-HBPE in distilled water, respectively.

of GO-HBPE slightly increases from 0.91 to 0.98. This implies that the surface of GO forms new defects and polar groups. So HBPE molecules are successfully attached on the surface of GO. The I_D/I_G ratio sharply decreases from 0.98 for GO-HBPE to 0.39 for RGO-HBPE, demonstrating that considerable defects derived from the oxygen-containing groups have been removed. In addition, the GO-HBPE and RGO-HBPE with similar shape and position for D and G bands suggest that the reduction process and decoration via HBPE did not destroy or change the structure of GO.

3.2. Dispersibility analysis

Fig. 2c and d shows the concentration versus time of GO-HBPE and RGO-HBPE dispersed in 20 mL DI water, respectively. Their dispersity was observed at different settling time intervals. In Fig. 2c and d, the concentration of GO-HBPE and RGO-HBPE is decreased by 2.1 and 5.0% due to the settling of the graphene particles, respectively. Both tend to be stable after placing for 120 h. Overall, both exhibit a stable and homogenous system in DI water, which is significant for further fabricating the graphene-based composites [17]. This expected result is ascribed to the oxygenic groups in the HBPE. In addition, the interaction between HBPE and water retards the graphene settlement and enhances their stable dispersion in water. This result indicates that the covalently bounded HBPE improves the dispersion of graphene in water. However, it should be noted that the stability of RGO-HBPE in water is slightly worse than that of GO-HBPE. This is because the reduction process decreases the hydrophilic oxygen-containing groups of HBPE and destroys some HBPE structures.

3.3. Rheology analysis

It has been reported that multiwall carbon nanotubes attached with HBPE via an ionic bond formed the nanoscale ionic materials with fluidity [8,14]. It is expected that both GO-HBPE and RGO-HBPE also exhibit definite liquid-like behaviors (Fig. S4b). However, as shown in Fig. S4b, the fact is that RGO-HBPE is a homogeneous viscous liquid while the GO-HBPE shows solid-like phase at room temperature. In order to explain this phenomenon, the rheological behaviors (loss (G'') and storage (G') modulus) for RGO-HBPE were assessed. As shown in Fig. 3a, the G' and G'' reasonably decrease gradually with increasing the temperature. Furthermore, it could be easily found that the value of G' is lower than that of G'' in the range of testing temperature, which indicates a liquid behavior [47,48]. In addition, it should be noted that the viscosity of RGO-HBPE also decreases with the rise of temperature (Fig. 3b), demonstrating more prominent flowability of RGO-HBPE after slight heating. In contrast, the resultant GO-HBPE always exhibited a solid-like manner even when it was heated, thus it was not evaluated by the rheological measurements in this work. Soft polymeric chains of HBPE are grafted on to RGO to move and thus lead to the fluidity for RGO-HBPE. Also, the reduction process slightly damages the grafting sites between RGO and HBPE (see Fig. S3), cuts some of the soft polymeric chains into smaller segments and releases part of crosslinking networks in the RGO-HBPE, which result in a liquid-like behavior for RGO-HBPE. Evidently, a high organic fraction (88.75 wt%) was verified in the RGO-HBPE liquids from the TGA test and thus acted as the fluid medium to warrant fluidity (see Fig. S5) [18,49]. For the GO-HBPE, the strong adsorption and the crosslinking networks of the substantial oxygen and polar functional groups in the soft polymeric chains contribute to the solid-like manner.

3.4. Tribological performance analysis

3.4.1. The effect of fluidity of RGO-HBPE

The GO-HBPE and RGO-HBPE exhibit different rheological manners in the above results. Herein, the effects of rheological behavior of GO-HBPE and RGO-HBPE on the tribological property were explored. The results are showed in Fig. 4a. To make a better comparison, the weights of GO-HBPE and RGO-HBPE in each steel plate were strictly controlled at 0.1 g. The blank steel plate was also performed for comparison. The friction coefficient of blank plate increases gradually as the time goes on (Fig. 4a). The detailed reason is that the elastic deformation at the contact area becomes more serious under a larger applied load, which push some fragments into a deeper depression. Thus, it consumes more energy and finally results in a higher friction coefficient with time elapsing. After the decoration of HBPE, the friction coefficient of GO-HBPE fluctuated heavily as exhibited in Fig. 4a. This unique phenomenon is attributed to the solid-like manner of GO-HBPE randomly dispersed on the surface of steel plate. In addition, GO-HBPE is inclined to flee to both sides during the friction process. Therefore, when the counterface ball comes across the steel plate coated with GO-HBPE, it is difficult for GO-HBPE to autonomously form the continuous film, leading to a larger friction coefficient and wider variation range. After the reduction procedure, the friction coefficient of RGO-HBPE shows the smallest value among those samples as shown in Fig. 4a. It is due to the formed lubricating film through spreading effect derived from the liquid-like behavior of RGO-HBPE [50]. As shown in Figs. 3 and 4S, RGO-HBPE is a homogeneous viscous liquid at room temperature, which can spontaneously flow and build the lubricating film on the steel plate. The formed lubricating film decreases the friction coefficient and reinforces antiwear by preventing direct contact and lowering the shear load between the steel plate and the counterface ball,

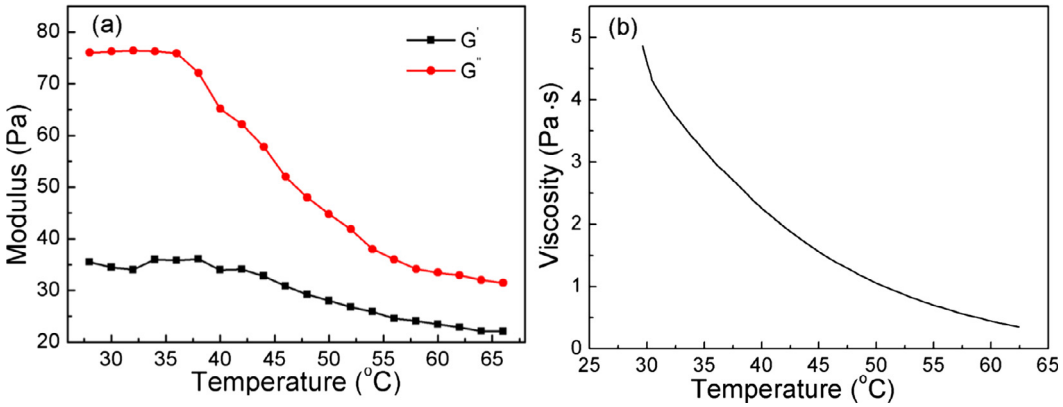

Fig. 3. Rheological response of RGO-HBPE: (a) G' and G'' Modulus and (b) viscosity versus temperature.

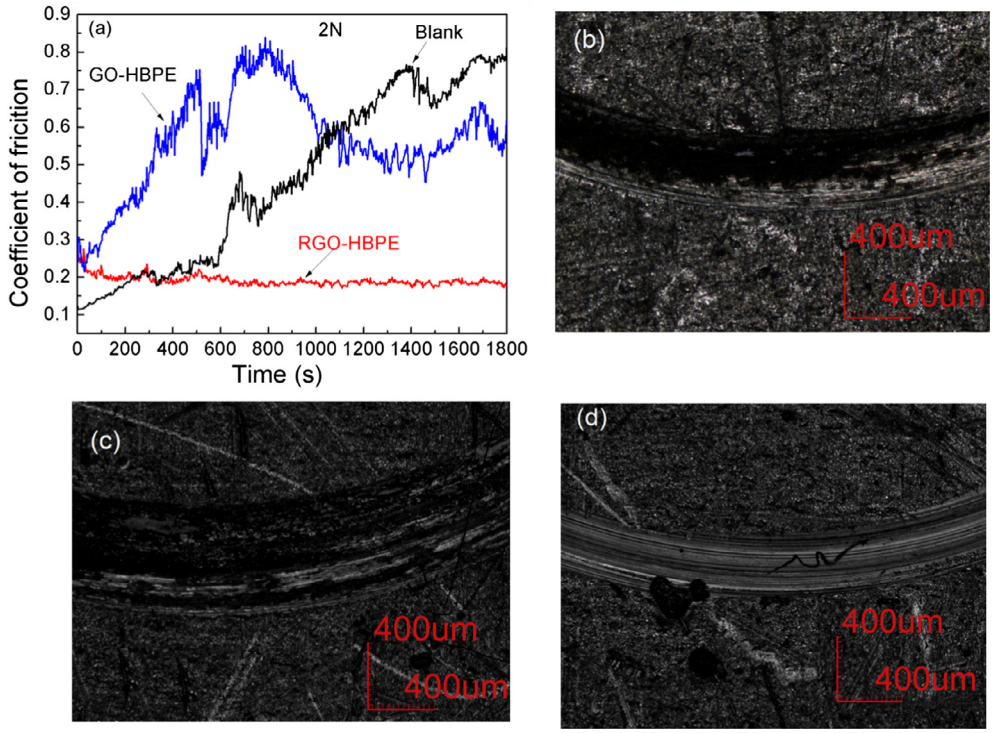

Fig. 4. Friction coefficient (a) and scanning microphotographs of worn surfaces of steel plate (b), plate coated with GO-HBPE (c), and RGO-HBPE (d) tested at 2 N for 30 min.

which is similar to that of liquid lubricants. Furthermore, the friction coefficient and their fluctuation of the RGO-HBPE always remain the lowest in the whole friction process due to the formed lubricating film.

The 2D scanning microphotographs of worn surfaces for the samples were obtained to detect the effects of the fluidity behavior on the surface of abrasion. Both the blank steel plate and GO-HBPE exhibit rough scratches (Fig. 4b and c). Whilst, in the case of RGO-HBPE (Fig. 4d), the worn surfaces are smoother than those of blank steel and GO-HBPE. In addition, as shown in Fig. 4c, a grinding crack with the largest width and deepest depth occurs for the GO-HBPE. However, RGO-HBPE (Fig. 4d) exhibits the lowest width and the shallowest depth under the same load. Their worn surfaces were also observed by SEM. The blank steel plate exhibits rough worn surfaces (Fig. 5a and b), which are due to the adherence wear resulting from the elastic or plastic deformation on the contact bump of steel plate. The worn surface of steel plate coated with GO-HBPE shows wide furrows scratches, while they are hardly found in the steel plate coated with RGO-HBPE (Fig. 5c and d). More importantly, the worn surface along the frictional direction of the steel plate coated with RGO-HBPE is blacker than that of the steel plate coated with GO-HBPE, which may be due to the formed carbon membrane during the frictional process. To verify this conjecture, EDS of the worn surface was obtained (Fig. 5e and f). The results demonstrate that the samples coated with RGO-HBPE contain a higher carbon content than the counterpart of GO-HBPE. The GO-HBPE with a solid-like phase served as particles to generate the abrasive wear on the surface of friction pairs and then cut into the low hardness stainless steel plate, leading to the furrows effects [51,52]. For the RGO-HBPE with a liquid-like behavior, the high mechanical strength and self-lubrication of graphene promote the formation of carbon membrane, which main contributes to the high wear resistance. While HBPE with soft polymeric organic chains and good flexibility is easy to form unique viscous thin lubricating film during the friction process, the soft polymeric organic chains make the RGO-HBPE naturally enter into the sliding interphase and scratches of worn field, which prevents the direct contact between plate and friction pairs. For GO-HBPE, however, viscous particles lacking liquidity conversely weaken the lubricity of GO itself and easily destroy the lubricating film. Namely, the RGO-HBPE not only forms a lubricating carbon film but also affords an orderly and viscous liquid film on the sliding interface to effectively isolate the direct rolling of ball on the metal plates, which is crucial to finally form a protective layer and thus gets a much smoother worn surface and lower friction coefficient [53,54].

3.4.2. The influence of applied load

Fig. 6 depicts the friction coefficient versus time under a constant applied load. The friction coefficient of the blank steel plate increases from 0.198 (1 N) to 0.673 (3 N). The increased 0.475 of friction coefficient is due to the generated deeper fovea arising from the larger elastic deformation under a larger applied load [55]. Thus, the friction pair has to fall into a deeper fovea in the sliding process, which increases the sliding distance and thus consumes a larger energy. Therefore, the blank steel plate exhibits a greater average friction coefficient for the larger applied load. For GO-HBPE, the friction coefficient initially increases, and then does not prominently change (in fact, a slight drop, Fig. 6b and d). The main reason is that the solid-like GO-HBPE is difficult to form a continuous lubricating film. Thus, the average friction coefficient increases at initial stage of loading. However, with continuously increasing the applied load, some compacted GO-HBPE form the solid-like lubricants to slightly decline the friction coefficient. As for RGO-HBPE (Fig. 6c and d), its friction coefficient is close to 0.2, which is much lower than those of blank steel and GO-HBPE. As shown in Fig. 6c, under the low applied load (such as 1 N), the friction coefficient of RGO-HBPE gradually declines as time goes on. In comparison, under the high applied load (such as 2 and 3 N), their friction coefficients are close to 0.2 with a little fluctuation during the whole friction testing process. Those completely different experimental phenomena are attributed to the lubricat-

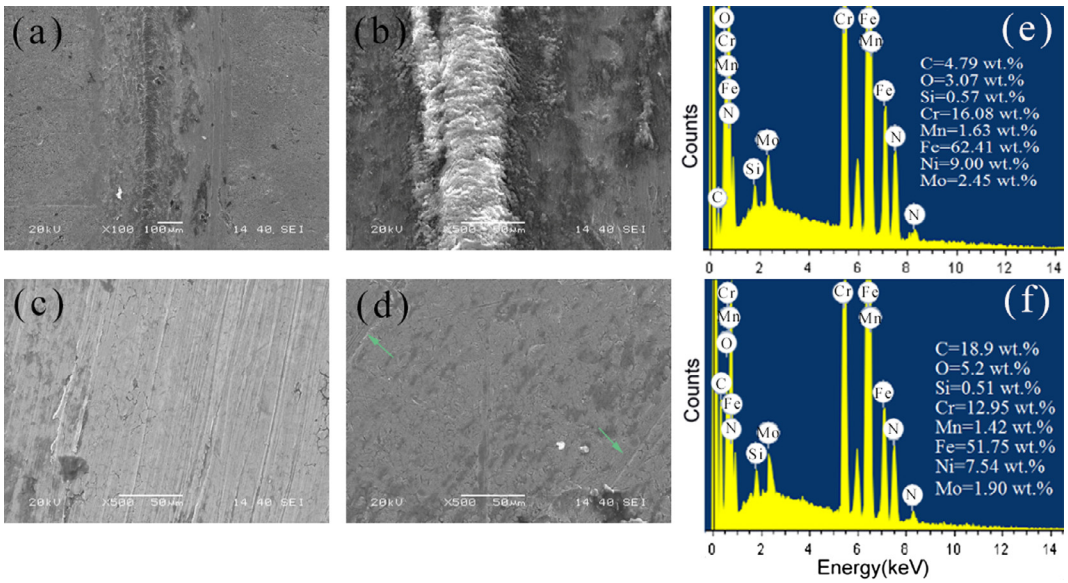

Fig. 5. Scanning electron microscope (SEM) images of worn surfaces of steel plates: blank (a, b), GO-HBPE (c), RGO-HBPE (d) and energy dispersive X-ray (EDX) spectrums GO-HBPE (e), RGO-HBPE (f) tested at 2 N for 30 min.

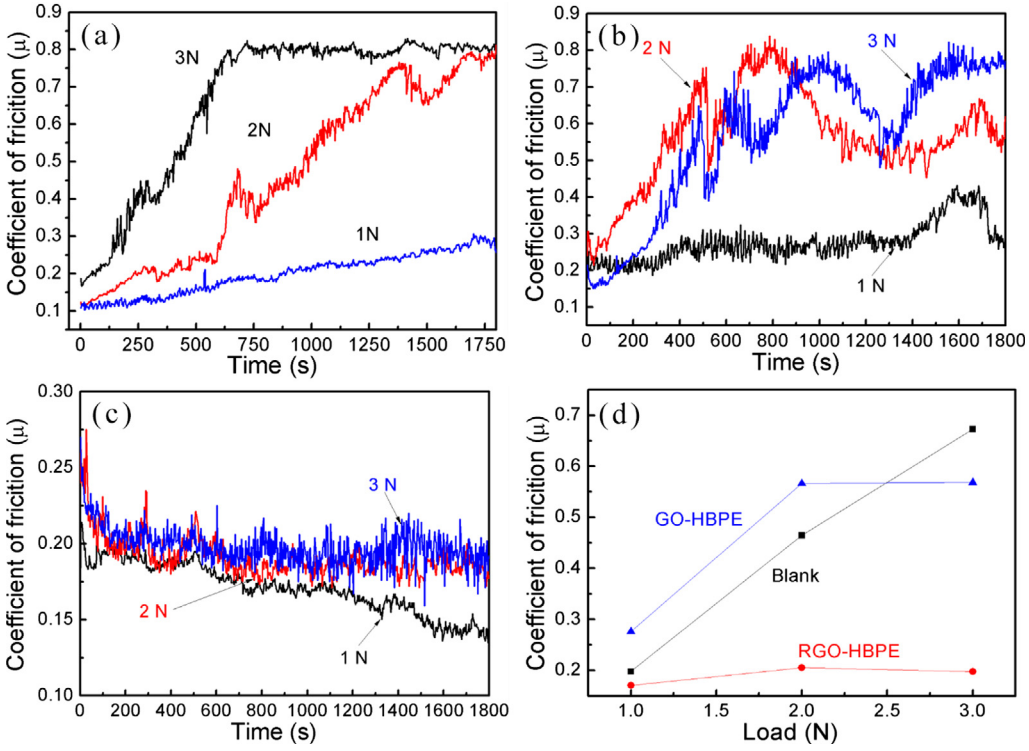

Fig. 6. The effect of the applied load on the friction coefficient of steel plates: blank (a), GO-HBPE (b) and RGO-HBPE (c), respectively, tested for 30 min. (d) The average friction coefficient curves of those three steel plate samples versus the applied load.

ing film. The RGO-HBPE can spontaneously flow and form the lubricating film through the spreading effect derived from its liquid-like behavior. In addition, the flowing of HBPE and graphene core oriented along the shear force direction and thus promoted the formation of lubricating film. Under the low applied load, the orientation of RGO-HBPE is not so easy that it cannot form a perfect lubricating film in a short time. Thus, the friction coefficient cannot sharply but gradually decrease as time goes on at 1 N. As for the high applied load, the orientation of RGO-HBPE becomes easier. Thus, a perfect lubricating film can be easily obtained in a short time, leading to a low friction coefficient with small fluctuation.

Fig. 7a and b presents the 2D scanning microphotographs of worn surfaces for RGO-HBPE with different applied loads. The worn surface of the steel plate coated with RGO-HBPE differs from that of the blank steel plate (Fig. 4b). RGO-HBPE always exhibits similar and smooth worn surfaces under each applied load (Fig. 4d, Fig. 7a and b). The only difference among them is their roughness and abrasion loss (Fig. 7c and d). For GO-HBPE, some

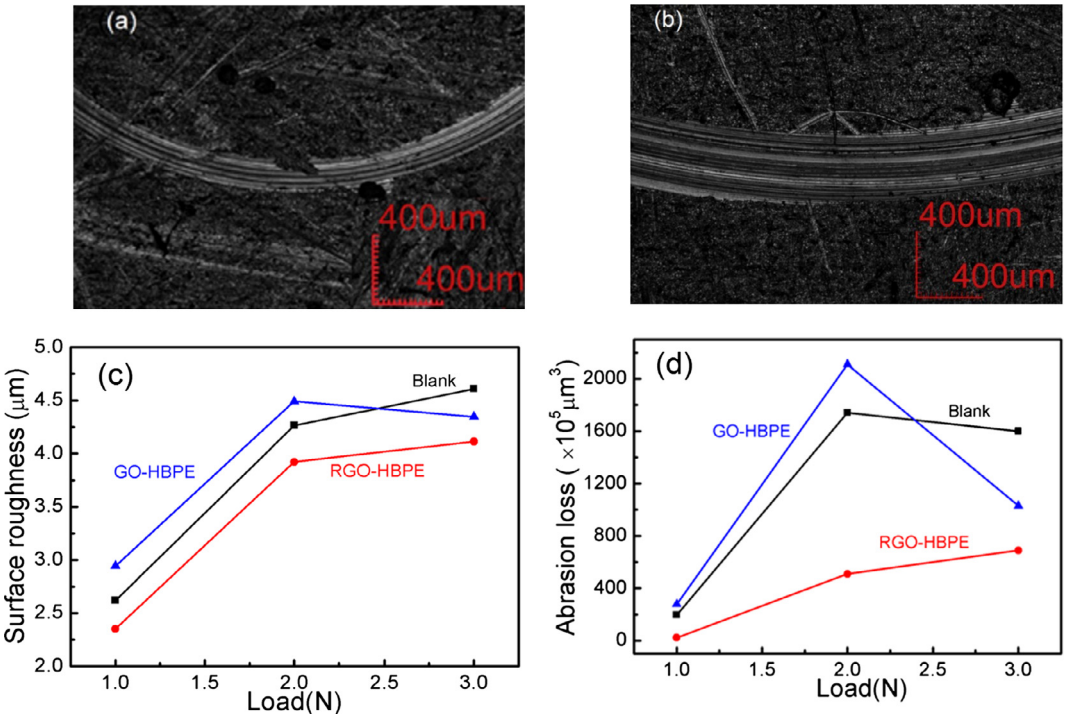

Fig. 7. Scanning microphotographs (2D) of worn surfaces of steel plates coated with RGO-HBPE tested at 1 N (a) and 3 N (b), respectively, for 30 min; The effect of the applied load on the surface roughness (c) and abrasion loss (d) of steel plates coated with different graphene materials tested for 30 min.

fragments coming from large plastic deformation cut the depressions by the later repeated sliding ball, which leads to a high abrasion loss (Fig. 7d). It is clear that the roughness and abrasion loss of the steel plate coated with RGO-HBPE firstly rise sharply and then begin to increase slowly, but are evidently lower than those of the steel plate coated with GO-HBPE and blank plate. This result can be understood by considering that the formed perfect lubricating film fills in the defects and traces on the friction pair, isolating the friction pair surface and providing the effect of lubricating. Most importantly, as shown in Figs. 6d and 7c & d, once the perfected lubricating film of RGO-HBPE is formed, the antifriction and antiwear of metal plate sharply increase.

3.5. Antifriction and lubricating mechanism for RGO-HBPE

From the above observations, a typical schematic of friction-reducing and lubricating mechanism of GO-HBPE and RGO-HBPE is proposed for the ball-plate sliding process as shown in Fig. 8 [56,57]. For the GO-HBPE case, as shown in Fig. 8a, when the ball rolls over the tray, there is no formation of lubricating film between the steel plate and the counterface ball. As shown in Figs. 1, 3 and S4, the GO-HBPE is a solid-like material. Thus, its spreading effect on the steel plate is not so good that it inclines to flee on either side during the friction process. In addition, although some of the GO-HBPE may be compacted and thus produce the effects of solid-like lubricating film, this kind of lubricating film is discontinuous and easy to be peeled off. Therefore, it is difficult to build an efficient protective cover on the sliding contact surfaces. In contrast, the soft polymeric HBPE serves as the base oil and the RGO acts as the additive for the RGO-HBPE system. HBPE is covalently grafted onto the RGO, forming a self-suspended system and advoiding the incompatibility between liquid and solid phases. Fig. 8b draws the lubricating mechanism of RGO-HBPE where the complex lubricating thin film is formed during the friction process. RGO-HBPE as the homogenous viscous liquid (Figs. 1, 3 and S4) can spontaneously flow and form a uniform absorbed film [58]. In

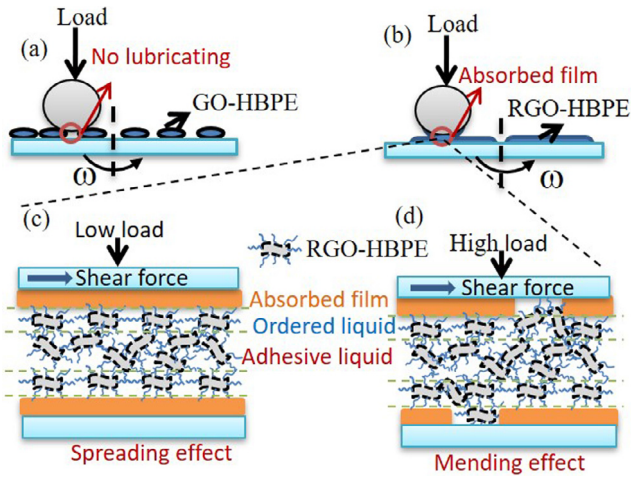

Fig. 8. The friction-reducing and lubricating mechanism for GO-HBPE and RGO-HBPE: GO-HBPE(a), RGO-HBPE(b), RGO-HBPE under low load (c) and under high load (d).

addition, the rolling ball accelerates the film to become very thin and actually plays the lubricating role [56]. For the low load case (such as 1 N) as shown in Fig. 8c, the formed absorbed film alleviates the wear and reduces the friction coefficient arising from the spreading effect. In addition, for RGO-HBPE, the directional movement along the shear force perfects the ordered liquid film and also contributes to a lower friction coefficient throughout the whole working time (Fig. 6c). Furthermore, under the high load (such as 2 and 3 N) as shown in Fig. 8d, the adhesive liquid film of RGO-HBPE is also favorable to spread graphene on the sliding contact surface and broken membrane area. Under the high load, the orientation of this RGO-HBPE liquids becomes easier to form the lubricating film in a short friction time, leading to a faint fluctuation for the friction coefficient. It is also easy to seep into the wear scars

and tracks under the high load. Most importantly, the high mechanical strength and self-lubricating properties of graphene core mainly contribute to the wear resistance [50,53,54]. Namely, the complex lubricating thin film from RGO-HBPE provides an isolated layer and also exhibits a mending effect for the broken membrane under the high load, which interprets the desired antiwear performance as shown in Figs. 6d and 7. Therefore, the synergistic effect between HBPE film and lubricating graphene endows RGO-HBPE liquids excellent antifriction properties.

4. Conclusions

For the previously reported solid and liquid lubricants with deficiencies, new methods have been taken to reduce the friction and wear [7,59,60]. Solvent-free nanomaterial liquids have attracted significant interests in the tribology field due to their desired designability and fluidity [12,61,62]. In this work, the chemical modification of GO and the reduction process were used to produce homogeneous viscous graphene liquids (RGO-HBPE) at room temperature, which exhibited a good dispersibility and stability in DI water and overcome easy agglomeration and incompatibility of solid lubricate in the liquid oil [24]. For the friction behavior of three samples, RGO-HBPE is the most favorable for lubrication and exhibits the smallest friction coefficient that is similar to graphene liquids based on M2070 block copolymers [62]. The friction coefficients for RGO-HBPE remain almost constant with increasing the applied load. But the value of other two samples rises significantly. Those excellent results could be understood by considering a spreading effect derived from the liquid-like behavior and a synergistic effect coming from the viscous thin film lubrication of HBPE and nano-lubrication of graphene. Therefore, the RGO-HBPE liquids are promising lubricants to be used without any base oil.

Acknowledgement

The authors acknowledge the National Natural Science Foundation of China (No. 51402132), the Shaanxi International Science and Technology Cooperation and Exchange Program (No. 2016KW-053), Jiangsu Government Scholarship for Overseas Studies (No. JS-2016-136), and Jiangsu Provincial Natural Science Foundation of China (BK20150466).

Appendix A. Supplementary material

Supplementary data to this article can be found online at https://doi.org/10.1016/j.jcis.2019.01.135.

References

[1] X. Li, H. Lu, J. Guo, Z. Tong, G. Dong, Synergistic water lubrication effect of self-assembled nanofilm and graphene oxide additive, Appl. Surf. Sci. 455 (2018) 1070–1077.
[2] H. Li, S. Li, F. Li, Z. Li, H. Wang, Fabrication of SiO_2 wrapped polystyrene microcapsules by Pickering polymerization for self-lubricating coatings, J. Colloid Interf. Sci. 528 (2018) 92–99.
[3] D. Berman, A. Erdemir, A.V. Sumant, Few layer graphene to reduce wear and friction on sliding steel surfaces, Carbon 54 (2013) 454–459.
[4] X. Sun, M. Zhao, B. Han, H. Kang, Z. Fan, Y. Liu, A. Umar, Z. Guo, Frictional reduction with partially exfoliated multi-walled carbon nanotubes as water-based lubricant additives, J. Nanosci. Nanotechno. 17 (2017) 1–6.
[5] J. Song, J. Zhang, C. Lin, Influence of graphene oxide on the tribological and electrical properties of PMMA composites, J. Nanomater. 6 (2013) 846102.
[6] Z.J. Zhang, D. Simionesie, C. Schaschke, Graphite and hybrid nanomaterials as lubricant additives, Lubricants 2 (2) (2014) 44–65.
[7] K. Fan, J. Liu, X. Wang, Y. Liu, W. Lai, S. Gao, J. Qin, X. Liu, Towards enhanced tribological performance as water-based lubricant additive: Selective fluorination of graphene oxide at mild temperature, J. Colloid Interf. Sci. 531 (2018) 138–147.
[8] F. Zhou, Y. Liang, W. Liu, Ionic liquid lubricants: designed chemistry for engineering applications, Chem. Soc. Rev. 38 (9) (2009) 2590–2599.
[9] X. Wu, J. Liu, Q. Zhao, M. Zhang, G. Zhao, X. Wang, In situ formed ionic liquids in polyol esters as high performance lubricants for steel/steel contacts at 300 degrees C, ACS Sustain. Eng. 3 (9) (2015) 2281–2290.
[10] V. Jaiswal, R.B. Rastogi, R. Kumar, L. Singh, K.D. Mandal, Tribological studies of stearic acid-modified $CaCu_{2.9}Zn_{0.1}Ti_4O_{12}$ nanoparticles as effective zero SAPS antiwear lubricant additives in paraffin oil, J. Mater. Chem. A 2 (2) (2014) 375–386.
[11] R. Rodriguez, R. Herrera, L.A. Archer, E.P. Giannelis, Nanoscale ionic materials, Adv. Mater. 20 (22) (2008) 4353–4358.
[12] N.J. Fernandes, T.J. Wallin, R.A. Vaia, H. Koerner, E.P. Giannelis, Nanoscale ionic materials, Chem. Mater. 26 (1) (2014) 84–96.
[13] J. Zhang, S.H. Chai, Z.-A. Qiao, S.M. Mahurin, J. Chen, Y. Fang, S. Wan, K. Nelson, P. Zhang, S. Dai, Porous liquids: A promising class of media for gas separation, Angew. Chem. Int. Edit. 54 (3) (2015) 932–936.
[14] J. Zhang, S. Liu, C. Yan, X. Wang, L. Wang, Y. Yu, S. Li, Abrasion properties of self-suspended hairy titanium dioxide nanomaterials, Appl. Nanosci. 7 (8) (2017) 1–10.
[15] B. Hong, A.Z. Panagiotopoulos, Diffusivities, viscosities, and conductivities of solvent-free ionically grafted nanoparticles, Soft Matter 9 (26) (2013) 6091–6102.
[16] J. Lu, F. Yan, J. Texter, Advanced applications of ionic liquids in polymer science, Prog. Polym. Sci. 34 (5) (2009) 431–448.
[17] L. Wu, B. Zhang, H. Lu, C.Y. Liu, Nanoscale ionic materials based on hydroxyl-functionalized graphene, J. Mater. Chem. A 2 (5) (2014) 1409–1417.
[18] P. Li, Y. Zheng, R. Yang, W. Fan, N. Wang, A. Zhang, Flexible nanoscale thread of $MnSn(OH)_6$ crystallite with liquid-like behavior and its application in nanocomposites, Chemphyschem 16 (12) (2015) 2524–2529.
[19] J.X. Zhang, K.M. Jiang, Y.P. Zheng, F. Wu, Y.Q. Li, The preparation of solvent-free multiwall carbon nanotubes/silica hybrid nanomaterial with liquid-like behavior, Funct. Mater. Lett. 6 (2) (2013) 1350015.
[20] Y.J. Mai, M.P. Zhou, H.J. Ling, F.X. Chen, W.Q. Lian, X.H. Jie, Surfactant-free electrodeposition of reduced graphene oxide/copper composite coatings with enhanced wear resistance, Appl. Surf. Sci. 433 (2018) 232–239.
[21] P. Li, Y. Zheng, T. Shi, Y. Wang, M. Li, C. Chen, J. Zhang, A solvent-free graphene oxide nanoribbon colloid as filler phase for epoxy-matrix composites with enhanced mechanical, thermal and tribological performance, Carbon 96 (2016) 40–48.
[22] Z. Wang, R. Wei, J. Gu, H. Liu, C. Liu, C. Luo, J. Kong, Q. Shao, N. Wang, Z. Guo, Ultralight, highly compressible and fire-retardant graphene aerogel with self-adjustable electromagnetic wave absorption, Carbon 139 (2018) 1126–1135.
[23] Z. Wang, H. Zhu, N. Cao, R. Du, Y. Liu, G. Zhao, Superhydrophobic surfaces with excellent abrasion resistance based on benzoxazine/mesoporous SiO_2, Mater. Lett. 186 (2017) 274–278.
[24] D. Kim, L.A. Archer, Nanoscale organic-inorganic hybrid lubricants, Langmuir 27 (6) (2011) 3083–3094.
[25] J. Hou, C. Bao, S. Qu, X. Hu, S. Nair, Y. Chen, Graphene oxide membranes for ion separation: Detailed studies on the effects of fabricating conditions, Appl. Surf. Sci. 459 (2018) 185–193.
[26] Y. Huangfu, C. Liang, Y. Han, H. Qiu, P. Song, L. Wang, J. Kong, J. Gu, Fabrication and investigation on the Fe_3O_4/thermally annealed graphene aerogel/epoxy electromagnetic interference shielding nanocomposites, Compos. Sci. Technol. 169 (2019) 70–75.
[27] J. Gu, C. Liang, X. Zhao, B. Gan, H. Qiu, Y. Guo, X. Yang, Q. Zhang, D.Y. Wang, Highly thermally conductive flame-retardant epoxy nanocomposites with reduced ignitability and excellent electrical conductivities, Compos. Sci. Technol. 139 (2017) 83–89.
[28] A. Mohamed, T. Ardyani, S. Abu Bakar, M. Sagisaka, Y. Umetsu, J.J. Hamon, B.A. Rahim, S.R. Esa, H.P.S.A. Khalil, M.H. Mamat, S. King, J. Eastoe, Rational design of aromatic surfactants for graphene/natural rubber latex nanocomposites with enhanced electrical conductivity, J. Colloid Interf. Sci. 516 (2018) 34–47.
[29] W. Bollmann, J. Spreadborough, Action of graphite as a lubricant, Nature 186 (4718) (1960) 29–30.
[30] M. Belmonte, C. Ramirez, J. Gonzalez-Julian, J. Schneider, P. Miranzo, M. Isabel Osendi, The beneficial effect of graphene nanofillers on the tribological performance of ceramics, Carbon 61 (2013) 431–435.
[31] J. Gu, N. Li, L. Tian, Z. Lv, Q. Zhang, High thermal conductivity graphite nanoplatelet/UHMWPE nanocomposites, RSC Adv. 5 (46) (2015) 36334–36339.
[32] J. Lin, L. Wang, G. Chen, Modification of graphene platelets and their tribological properties as a lubricant additive, Tribol. Lett. 41 (1) (2011) 209–215.
[33] Y. Jiao, J. Zhang, S. Liu, Y. Liang, S. Li, H. Zhou, J. Zhang, The graphene oxide ionic solvent-free nanofluids and their battery performances, Sci. Adv. Mater. 10 (12) (2018) 1706–1713.
[34] Z. Xu, X. Shi, W. Zhai, J. Yao, S. Song, Q. Zhang, Preparation and tribological properties of TiAl matrix composites reinforced by multilayer graphene, Carbon 67 (2014) 168–177.
[35] Y. Guo, G. Xu, X. Yang, K. Ruan, T. Ma, Q. Zhang, J. Gu, Y. Wu, H. Liu, Z. Guo, Significantly enhanced and precisely modeled thermal conductivity in polyimide nanocomposites with chemically modified graphene via in situ polymerization and electrospinning-hot press technology, J. Mater. Chem. C 6 (12) (2018) 3004–3015.
[36] B. Kirubasankar, V. Murugadoss, J. Lin, T. Ding, M. Dong, H. Liu, J. Zhang, T. Li, N. Wang, Z. Guo, S. Angaiah, In situ grown nickel selenide on graphene

nanohybrid electrodes for high energy density asymmetric supercapacitors, Nanoscale 10 (43) (2018) 20414–20425.
[37] J. Zhang, Y. Zheng, P. Yu, S. Mo, R. Wang, The synthesis of functionalized carbon nanotubes by hyperbranched poly(amine-ester) with liquid-like behavior at room temperature, Polymer 50 (13) (2009) 2953–2957.
[38] Z. Yang, X. Hao, S. Chen, Z. Ma, W. Wang, C. Wang, L. Yue, H. Sun, Q. Shao, V. Murugadoss, Long-term antibacterial stable reduced graphene oxide nanocomposites loaded with cuprous oxide nanoparticles, J. Colloid Interf. Sci. 533 (2019) 13–23.
[39] X. Wang, X. Liu, H. Yuan, H. Liu, C. Liu, T. Li, C. Yan, X. Yan, C. Shen, Z. Guo, Non-covalently functionalized graphene strengthened poly(vinyl alcohol), Mater. Design 139 (2018) 372–379.
[40] Z. Guo, Y. Qian, Y. Yuan, H. Wang, H. Liu, J. Zhang, S. Shi, N. Wang, Highly efficient uranium adsorption by salicylaldoxime/polydopamine graphene oxide nanocomposites, J. Mater. Chem. A 6 (48) (2018) 24676–24685.
[41] R.K. Srivastava, V.S.M. Vemuru, Y. Zeng, R. Vajtai, S. Nagarajaiah, P.M. Ajayan, A. Srivastava, The strain sensing and thermal-mechanical behavior of flexible multi-walled carbon nanotube/polystyrene composite films, Carbon 49 (12) (2011) 3928–3936.
[42] P. Li, Y. Zheng, Y. Wu, P. Qu, R. Yang, A. Zhang, Nanoscale ionic graphene material with liquid-like behavior in the absence of solvent, Appl. Surf. Sci. 314 (2014) 983–990.
[43] L. Guadagno, B. De Vivo, A. Di Bartolomeo, P. Lamberti, A. Sorrentino, V. Tucci, L. Vertuccio, V. Vittoria, Effect of functionalization on the thermo-mechanical and electrical behavior of multi-wall carbon nanotube/epoxy composites, Carbon 49 (6) (2011) 1919–1930.
[44] M. Idrees, S. Batool, J. Kong, Q. Zhuang, H. Liu, Q. Shao, N. Lu, Y. Feng, E.K. Wujcik, Q. Gao, Polyborosilazane derived ceramics - Nitrogen sulfur dual doped graphene nanocomposite anode for enhanced lithium ion batteries, Electrochim. Acta 296 (2019) 925–937.
[45] Y. Zhang, L. Qian, W. Zhao, X. Li, X. Huang, X. Mai, Z. Wang, Q. Shao, X. Yan, Z. Guo, Highly efficient Fe-N-C nanoparticles modified porous graphene composites for oxygen reduction reaction, J. Electrochem. Soc. 165 (9) (2018).
[46] W. Deng, T. Kang, H. Liu, J. Zhang, N. Wang, N. Lu, Y. Ma, A. Umar, Z. Guo, Potassium hydroxide activated and nitrogen doped graphene with enhanced supercapacitive behavior, Sci. Adv. Mater. 10 (7) (2018) 937–949.
[47] S.A. Kim, R. Mangal, L.A. Archer, Relaxation dynamics of nanoparticle-tethered polymer chains, Macromolecules 48 (17) (2015) 6280–6293.
[48] Q. Li, L. Dong, F. Sun, J. Huang, H. Xie, C. Xiong, Self-unfolded graphene sheets, Chem. Eur. J. 18 (23) (2012) 7055–7059.
[49] Q. Li, L. Dong, W. Deng, Q. Zhu, Y. Liu, C. Xiong, Solvent-free fluids based on rhombohedral nanoparticles of calcium carbonate, J. Am. Chem. Soc. 131 (26) (2009) 9148–9149.
[50] C. Liu, H. Yan, Q. Lv, S. Li, S. Niu, Enhanced tribological properties of aligned reduced graphene oxide-Fe_3O_4@polyphosphazene/bismaleimides composites, Carbon 102 (2016) 145–153.
[51] L. Wang, Y. Liu, W. Si, H. Feng, Y. Tao, Z. Ma, Friction and wear behaviors of dental ceramics against natural tooth enamel, J. the Eur. Ceram. Soc. 32 (11) (2012) 2599–2606.
[52] D. Berman, S.A. Deshmukh, S.K. Sankaranarayanan, A. Erdemir, A.V. Sumant, Macroscale superlubricity enabled by graphene nanoscroll formation, Science 348 (6239) (2015) 1118–1122.
[53] C. Liu, H. Yan, Z. Chen, L. Yuan, T. Liu, Enhanced tribological properties of bismaleimides filled with aligned graphene nanosheets coated with Fe_3O_4 nanorods, J. Mater. Chem. A 3 (19) (2015) 10559–10565.
[54] P. Li, R. Yang, Y. Zheng, P. Qu, L. Chen, Effect of polyether amine canopy structure on carbon dioxide uptake of solvent-free nanofluids based on multiwalled carbon nanotubes, Carbon 95 (2015) 408–418.
[55] L.J. Cui, H.Z. Geng, W.Y. Wang, L.T. Chen, J. Gao, Functionalization of multi-wall carbon nanotubes to reduce the coefficient of the friction and improve the wear resistance of multi-wall carbon nanotube/epoxy composites, Carbon 54 (2013) 277–282.
[56] S. Liang, Z. Shen, M. Yi, L. Liu, X. Zhang, S. Ma, In-situ exfoliated graphene for high-performance water-based lubricants, Carbon 96 (2016) 1181–1190.
[57] B. Wang, W. Tang, H. Lu, Z. Huang, Ionic liquid capped carbon dots as a high-performance friction-reducing and antiwear additive for poly(ethylene glycol), J. Mater. Chem. A 4 (19) (2016) 7257–7265.
[58] S. Gu, Y. Zhang, B. Yan, Solvent-free ionic molybdenum disulfide (MoS_2) nanofluids with self-healing lubricating behaviors, Mater. Lett. 97 (2013) 169–172.
[59] J. Akilavasan, K. Wijeratne, A. Gannoruwa, A.R.M. Alamoud, J. Bandara, Significance of $TiCl_4$ post-treatment on the performance of hydrothermally synthesized titania nanotubes-based dye-sensitized solar cells, Appl. Nanosci. 4 (2) (2014) 185–188.
[60] R. Gusain, H.P. Mungse, N. Kumar, T.R. Ravindran, R. Pandian, H. Sugimura, O.P. Khatri, Covalently attached graphene-ionic liquid hybrid nanomaterials: synthesis, characterization and tribological application, J. Mater. Chem. A 4 (3) (2016) 926–937.
[61] J.X. Zhang, J. Yi, Y.T. Jiao, S.Y. Li, X.L. Shi, K. Sun, Preparation and application of water-soluble tio2-ionic liquids hybrid nanomaterials, J. Inorg. Mater. 33 (5) (2018) 577–581.
[62] J. Yang, Y.F. Xia, H.J. Song, B.B. Chen, Z.Z. Zhang, Synthesis of the liquid-like graphene with excellent tribological properties, Tribol. Int. 105 (2017) 118–124.